IGARSS 2023 - 2023 IEEE International Geoscience and Remote Sensing Symposium | 979-8-3503-2010-7/23/$31.00 ©2023 IEEE | DOI: 10.1109/IGARSS52108.2023.10283450

EARLY DISEASE DETECTION WITH HYPERSPECTRAL IMAGERY: DYNAMICS OF PLANT TRAITS AS A FUNCTION OF DISEASE SEVERITY LEVELS

T. Poblete[1,2], A. Hornero[2,3], V. Gonzalez-Dugo[3], B.B. Landa[3], J.A. Navas-Cortes[3], P.J. Zarco-Tejada[1,2,3]

[1]School of Agriculture, Food and Ecosystem Sciences (SAFES), Faculty of Science (FoS), The University of Melbourne, Melbourne, Victoria, Australia
[2]Faculty of Engineering and Information Technology (FEIT), The University of Melbourne, Melbourne, Victoria, Australia
[3]Instituto de Agricultura Sostenible (IAS), Consejo Superior de Investigaciones Científicas (CSIC), Menendez Pidal s/n, 14004 Córdoba, Spain

ABSTRACT

Traditional methods to identify biotic-induced plant stress are time-consuming and costly. Airborne hyperspectral and thermal imagery has shown promise in identifying disease symptoms caused by pathogens in several plant species. Specifically, to detect *Xylella fastidiosa* (*Xf*) and *Verticillium dahliae* (*Vd*), previous studies have aimed to detect symptomatic and asymptomatic trees with high accuracy. Nevertheless, these studies did not explore the progressive changes in plant traits with increasing disease severity levels. In this study, we investigate the dynamics of plant traits as a function of disease severity.

Moreover, we focus on the plant traits derived from hyperspectral data that contribute the most to disease detection, assessing how their role is redistributed as a function of disease severity. Finally, we evaluate the contribution of the plant traits in asymptomatic trees undetectable by visual inspection, using as a reference qPCR analysis. The findings revealed that specific traits such as the NPQI and PRIn indices and SIF and Anth were the most crucial.

Index Terms— Hyperspectral, Plant traits, Biotic stress detection, Disease progression.

1. INTRODUCTION

Conventional methods for biotic-induced plant stress detection require *in situ* monitoring techniques which are time-consuming and expensive. The large-scale detection using airborne hyperspectral and thermal imagery has helped to detect disease symptoms induced by pathogens in several host plant species [1-3]. In such studies, the prediction methods relied on detecting asymptomatic vs. symptomatic diseased trees. In particular, the discrimination between two pathogens triggering similar symptoms was achieved using a three-stage modeling approach [1], while disentangling abiotic vs. biotic sources of stress was achieved by identifying divergent plant traits [2]. Nevertheless, such studies focused on symptomatic (infected) vs. asymptomatic (healthy) trees via visual assessment and quantitative molecular polymerase chain reaction assays (qPCR), while the dynamics of the plant traits to track progressively increasing levels of infections have not been attempted. Previous tests suggested that the most sensitive trait expressed with increasing levels of disease severity on infected trees (i.e., initial vs. advanced stages) was solar-induced fluorescence (SIF) emission. At the same time, the importance of CWSI decreased after the initial disease severity stage. These results demonstrated that understanding the dynamics of the plant traits as a function of increasing levels of biotic stress could play a key role in understanding the physiological changes of infected vegetation. Therefore, in this study, we investigated the dynamics of the plant traits as a function of disease severity levels. Moreover, we

Authorized licensed use limited to: University of Melbourne. Downloaded on October 23,2023 at 00:34:09 UTC from IEEE Xplore. Restrictions apply.

focus on the plant traits derived from hyperspectral data that contribute the most to disease detection, assessing how their role is redistributed as a function of disease severity. Finally, we compared the contribution of the plant traits to determine their role in cases of asymptomatic infections undetectable by visual disease assessment. This analysis was performed by comparing trees whose infection by the pathogen tested by qPCR were negative and assessed as asymptomatic (true negatives) against trees tested positive by qPCR that were evaluated as asymptomatic by the naked eye (false negatives).

2. MATERIALS AND METHODS

2.1. Airborne hyperspectral imagery and visual assessment of the infection

2.1.1. Visual assessment and qPCR analysis of infected trees

Visual assessment of olive trees infected with *Xylella fastidiosa* (*Xf*) or *Verticillium dahliae* (*Vd*) in outbreak zones was conducted in Italy and Australia, respectively. Visual assessments of the disease severity were performed, where trees without visible symptoms were evaluated as asymptomatic (SEV=0), and trees with visual symptoms were assessed using a scale of 1–4 based on the extent of foliar symptoms.

In Apulia, Italy, 7,296 olive trees were assessed during 2016 and 2017, where 4,045 were reported as asymptomatic and 3,251 as symptomatic (45%, SEV = 1; 41%, SEV = 2; 11%, SEV = 3; and 3%, SEV = 4). In the Mallee region, Victoria, Australia, 1,036 olive trees were assessed during 2020 and 2022, with 355 being asymptomatic and 681 being symptomatic 42%, SEV = 1; 18%, SEV = 2; 23%, SEV = 3 and 17%, SEV = 4), on 2020-2021. While in 2021–2022, 1,296 olive trees were assessed, where 258 were reported as asymptomatic and 1,038 as symptomatic (23%, SEV = 1; 27%, SEV = 2; 27%, SEV = 3; and 23%, SEV = 4).

2.1.2. Airborne hyperspectral imagery collection and processing

Narrow-band hyperspectral data were collected over both study sites alongside field assessments. In Apulia, a Headwall Photonics VNIR linear hyperspectral sensor (Microhyperspec A-Series) captured 260 bands ranging from 400 to 885 nm with a 6.4-nm full-width at half maximum (FWHM). In the Mallee region, the hyperspectral imager (Hyperspec VNIR E-Series model, Headwall Photonics) captured 371 bands ranging from 400 to 1000 nm with a 5.8-nm FWHM. Radiometric calibration was performed on the hyperspectral imagery collected by both sensors, applying to each image the coefficients obtained from different illumination levels with a constant light source using a CSTM-USS-2000C and a SPARC-A060L integrating sphere (LabSphere, North Sutton, NH, USA) for the 6.4-nm and the 5.8-nm FWHM sensors, respectively. The atmospheric correction and irradiance calculation to convert radiance values to reflectance was conducted with the SMARTS model [4]. The aerosol optical depth at 550 nm was derived from readings obtained at various wavelengths using a Microtops II sun photometer (Solar LIGHT Co.), while meteorological parameters were obtained from portable weather stations (Transmitter PTU30 and WXT510, Vaisala, respectively).

The calibrated and atmospherically corrected hyperspectral images were ortho-rectified using PARGE (ReSe Applications Schläpfer, Wil, Switzerland), which utilized GPS/INS data synchronized onboard (IG500, SBG Systems, Carrières-sur-Seine, France, for Italy; VN-300, VectorNav Technologies LLC, Dallas, TX, USA, for Australia). Pure tree-crown radiance was used for the quantification of sun-induced chlorophyll fluorescence at 760 nm (SIF) using the O_2-A *in-filling* Fraunhofer Line Depth (FLD) method [5]. In addition, pure tree-crown reflectance was used to 1) calculate the set of narrow-band hyperspectral indices (NBHIs) and 2) to retrieve leaf biochemical and canopy structural parameters obtained by inversion of radiative transfer models (methodology described in section 2.2.1).

Authorized licensed use limited to: University of Melbourne. Downloaded on October 23,2023 at 00:34:09 UTC from IEEE Xplore. Restrictions apply.

2.2. Modelling methods

2.2.1. Plant traits quantification

Leaf pigments such as carotenoids (C_{x+c}), chlorophyll *a+b* (C_{a+b}), and anthocyanins (Anth.) and canopy structural properties, including leaf area index (LAI) and the leaf inclination distribution function (LIDF) were obtained by inverting radiative transfer models. The PRO4SAIL model was used to create a look-up table of 100,000 simulations. SVR algorithms were used to train models to invert the plant traits (more information can be found in [1-3]).

2.2.2. Disease detection and quantification of the contribution of plant traits

The detection of disease symptoms was performed by training RF algorithms to classify asymptomatic (SEV = 0) vs the following stages: i) early stage, which included trees assessed as symptomatic with SEV = 1; ii) middle stage, which included trees assessed as symptomatic with SEV= {1,2}; and iii) all levels of infection, which included all trees assessed as symptomatic SEV= {1,2,3,4}.

Following the methodology in [1,2], Random Forest (RF) algorithms were trained using a balanced dataset of asymptomatic trees and trees from the described three categories. The following plant traits were inputs to the RF model: C_{a+b}, Anth., C_{x+c}, LAI, LIDF, SIF and non-colinear NBHI. The latest was obtained by reducing their dimensionality and a subsequent recursive feature selection. The dimensionality of the NBHI pool of indices was reduced by the variance inflation factor (VIF) analysis, and indices with a VIF > 5 were removed. A recursive feature elimination approach was then performed, and the models did not include indices that did not improve the classification accuracies (OA) and the *kappa coefficients* (κ). Finally, the hyperparameters of the models were optimized using a Bayesian optimization method in MATLAB.

For each dataset, the importance of each predictor was determined using the permutation of the out-of-bag method [8]. Then, a further analysis was focused on the early stages of the infection by using the plant traits with the highest contribution.

3. RESULTS

The Normalized Phaeophytinization Index (NPQI), SIF, and the Normalized Photochemical Reflectance Index (PRIn), $C_{a+b,}$ and Anth were the plant traits that showed the highest relative importance in detecting all the stages of infection. NPQI and SIF showed an increase as a function of severity, while PRIn showed its highest importance for the early stages of the infection. Anth was stable across all levels of infection. For the detection of early stages of infection, indices and plant traits related to carotenoids such as CRI_{700M} and C_{x+c} contributed the least. Structural parameters such as LAI and $LIDF_a$ had their lowest contribution when detecting all stages of infection (Fig. 1).

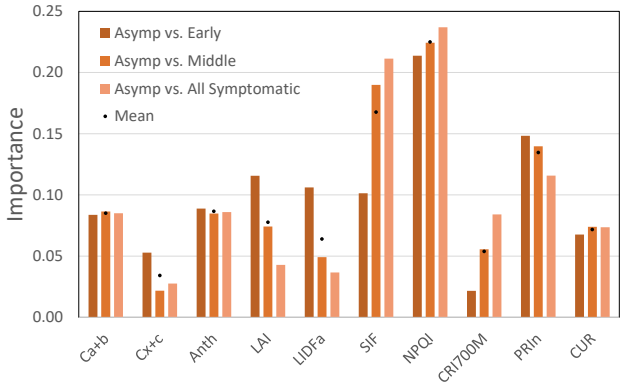

Fig. 1: Progression of the spectral plant traits' importance in detecting early, middle, and all symptomatic severity levels

Results when assessing only the most important traits showed a redistribution on their contribution (Fig. 2). We observed that both PRIn and NPQI had the highest and almost equal contribution. When PRIn was not included in the assessment, NPQI had the greatest contribution with more than double of the importance achieved by Anth. Notably, NPQI and Anth took the significance of SIF. These results are relevant because PRIn was shown to track xanthophyll cycle dynamics, a pigment indirectly related to NPQI and chlorophyll *a+b* degradation.

Authorized licensed use limited to: University of Melbourne. Downloaded on October 23,2023 at 00:34:09 UTC from IEEE Xplore. Restrictions apply.

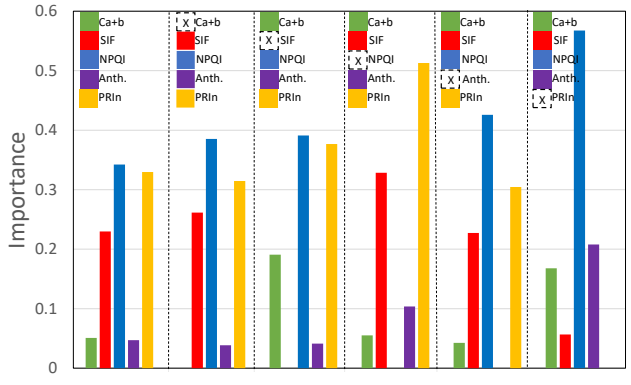

Fig. 2: Assessment of the most important plant traits' dynamics to detect early *Xylella fastidiosa* infection stages.

These results were confirmed by the true negative vs false positive analysis, where we observed that the plant trait that showed the highest contribution was Anth, closely followed by PRIn (Fig. 3). These plant traits played a complementary relationship. When Anth was removed, PRIn almost doubled its original contribution and vice versa. The remaining plant traits did not exhibit significant changes in their contributions.

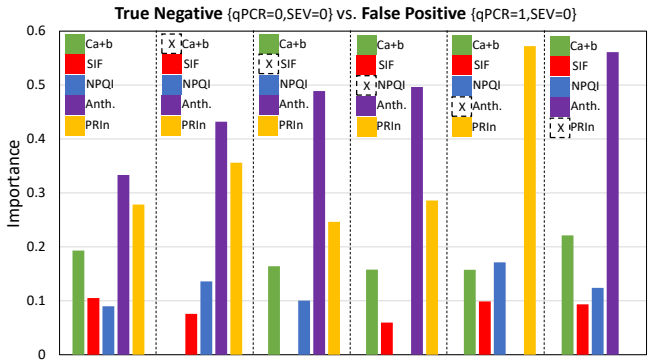

Fig. 3: Assessment of the most important plant traits for assessing True Negative vs False Positive rates from the qPCR analysis.

4. CONCLUSIONS

This study aimed to identify the contribution and the progression of the most sensitive spectral indices and traits for the detection of vascular pathogens affecting olive trees from hyperspectral imagery through the inversion of RTM using SVM algorithms. Results showed that the plant traits with the highest contribution were SIF, NPQI and Anth., and C_{a+b}. This was consistent with the False Positive vs True Negative results analysis comparing molecular qPCR assays and visual assessments.

5. REFERENCES

[1] Poblete, T., et al. "Discriminating Xylella Fastidiosa from Verticillium Dahliae Infections in Olive Trees Using Thermal- and Hyperspectral-Based Plant Traits." *ISPRS Journal of Photogrammetry and Remote Sensing*, vol. 179, pp. 144–133, Sept. 2021.

[2] Zarco-Tejada, P. J., et al. "Divergent Abiotic Spectral Pathways Unravel Pathogen Stress Signals across Species." Nature Communications, vol. 12, no. 1, pp. 1–11, Oct. 2021.

[3] Zarco-Tejada, P. J., et al. "Previsual Symptoms of *Xylella Fastidiosa* Infection Revealed in Spectral Plant-Trait Alterations." *Nature Plants*, vol. 4, no. 7, pp. 432–39, July 2018.

[4] Gueymard, Christian A. "Parameterized Transmittance Model for Direct Beam and Circumsolar Spectral Irradiance." Solar Energy, vol. 71, no. 5, Oct. 2001.

[5] Plascyk, James A. "Mk Ii Fraunhofer Line Discriminator (Fld-Ii) for Airborne and Orbital Remote Sensing of Solar-Stimulated Luminescence." Optical Engineering, vol. 14, no. 4, pp. 339–4. Jan. 1975

[6] Féret, J. B., et al. "PROSPECT-D: Towards Modeling Leaf Optical Properties through a Complete Lifecycle." *Remote Sensing of Environment*, vol. 2017, Jan. 2017

[7] Verhoef, W., et al. "Unified Optical-Thermal Four-Stream Radiative Transfer Theory for Homogeneous Vegetation Canopies." IEEE Transactions on Geoscience and Remote Sensing, Geoscience and Remote Sensing, IEEE Transactions on, IEEE Trans. Geosci. Remote Sensing, vol. 45, no. 6, pp. 1808–22, June 2007.

[8] Thomas, V. A., et al. "Mapping Thins to Identify Active Forest Management in Southern Pine Plantations Using Landsat Time Series Stacks." Remote Sensing of Environment, vol. 252, Jan. 2021.

Authorized licensed use limited to: University of Melbourne. Downloaded on October 23,2023 at 00:34:09 UTC from IEEE Xplore. Restrictions apply.